ADVANCED SENSOR RESEARCH
Open Access
www.advsensorres.com

Beyond the Passive Diffusion: Core@Satellite Magneto-Plasmonic Particles for Rapid and Sensitive Colorimetric Immunosensor Response

Maria De Luca, Adriano Acunzo, Daniele Marra, Margherita Borriello, Diego Ingrosso, Raffaele Velotta, Vincenzo Iannotti, and Bartolomeo Della Ventura*

Magneto-plasmonic particles, comprising gold and iron oxide, exhibit substantial potential for biosensing applications due to their distinct properties. Gold nanoparticles (AuNPs) provide plasmonic features, while iron oxide composites, responsive to an external magnetic field, significantly reduce detection time compared to passive diffusion. This study explores core@satellite magneto-plasmonic particles (CSMPs), featuring magnetic nanoparticle clusters and numerous satellite-like AuNPs, to amplify the optical response on a nanostructured gold surface. Using a sandwich scheme, target analytes are detected as hybrid nanoparticles bind to the pre-immobilized target on the AuNPs surface, inducing changes in the immunosensor's extinction spectrum. Application of an external magnetic field notably enhances biosensor response and sensitivity, reducing assay time from hours to minutes. Leveraging the properties of CSMPs, the immunosensor detects specific immune protein at low concentrations within minutes. CSMPs hold considerable promise for precise and sensitive analyte detection, offering potential applications in rapid testing and mass screening.

1. Introduction

In recent years, magneto-plasmonic nanoparticles have gained significant attention in biosensing, emerging as versatile tools for detecting and analyzing biological molecules.[1–5] These nanoparticles combine the key characteristics of two crucial phenomena: plasmonics exhibited by metal nanoparticles (NPs) and magnetic properties of nanocrystals of 3d metals and their oxides.[6,7] The outstanding optical properties of metal NPs primarily arise from the localized surface plasmon resonance (LSPR) effect.[8] This phenomenon results from the collective oscillations of surface electrons induced by visible light, leading to an extinction band in the visible region of the optical spectrum.[9,10] The resonance wavelength of LSPR can be adjusted by manipulating the size, shape, and composition of the NPs, as well as the distance between them and the refractive index of the surrounding medium. LSPR's adaptability makes it a powerful tool for biosensing, as the binding of biomolecules to the NP surface induces a shift in the resonance wavelength, detectable and quantifiable.[6] Gold NPs (AuNPs) are preferred in this context due to their exceptional optical properties and biocompatibility, boasting a non-toxic and chemically stable surface under physiological conditions.[11,12]

On the other hand, the effectiveness of controlling functionalized materials using magnetic nano/microparticles through the use of an external magnetic field is well known.[13] The widely used magnetic material is iron oxide composite Fe_3O_4, which shows superparamagnetism for a NP diameter less than 20 nm.[14] Magnetic NP (MNP) clusters are frequently utilized, offering an enhanced and cooperative magnetic response that results in improved saturation magnetization and reduced coercive field at low temperatures.[15,16] Despite their size, the functionalization of magnetic surfaces involves lengthy biochemical procedures, posing challenges for scalability in industrial applications. Combining MNP clusters with a gold structure offers the advantages of robust gold surface chemistry and the unique properties of MNP clusters. Furthermore, this

M. De Luca, A. Acunzo, D. Marra, R. Velotta, V. Iannotti, B. Della Ventura
Department of Physics "E. Pancini"
University of Naples Federico II
Via Cintia 26, Napoli 80126, Italy
E-mail: raffaele.velotta@unina.it

M. Borriello, D. Ingrosso
Department of Experimental Medicine
University of Campania Luigi Vanvitelli
Via de Crecchio 7, Napoli 80138, Italy

V. Iannotti
Institute for Superconducting
Oxides and other Innovative Materials and Devices of the National Research Council (CNR-SPIN)
Piazzale V. Tecchio 80, Napoli 80125, Italy

The ORCID identification number(s) for the author(s) of this article can be found under https://doi.org/10.1002/adsr.202400006

DOI: 10.1002/adsr.202400006

configuration can protect the magnetic core from oxidation and corrosion. As an optimal coating, strategically distributed gold spots on the surface streamline the functionalization process for linking bioreceptors,[17] relying on gold's surface chemistry and biocompatibility, while a fragmented rather than uniform gold coating preserves the magnetic properties. Considerable attention has been devoted to strategies for fabricating multifunctional magneto-plasmonic nanostructures,[18–21] leading to the development of several immunosensors.[22–24] Utilizing the innovative properties of magneto-plasmonic materials, these NPs can function as amplifiers to enhance the optical response of a plasmonic nanostructured surface. Simultaneously, the magnetic properties contribute to the acceleration of the detection time. In a recent study, Gessner et al. utilized magnetic AuNPs with an idealized coating (MAGIC) in a sandwich scheme to amplify the LSPR shift on a plasmonic surface composed of Au nanobipyramids.[25] The application of a zwitterionic polymer coating conferred nearly neutral charge properties to MAGIC NPs, effectively minimizing nonspecific protein adsorption.[26] However, the polymer created a spatial gap between the NPs and the nanostructured surface. To enhance plasmonic coupling between the Au nanobipyramids surface and MAGIC NPs, a half-antibody was utilized. With an LSPR shift ranging from 0 to 6 nm at analyte concentrations between 10^{-3} and 10^{3} ng mL^{-1}, MAGIC NPs enable the detection of specific molecular urinary biomarkers in the presence of other proteins at levels as low as a few dozen pg mL^{-1} within minutes. With this conceptual framework in mind, we employed core@satellite magneto-plasmonic particles (CSMPs), which consist of a Fe_3O_4 NPs cluster (diameter ≈ 250 nm) decorated with AuNPs (≈20 nm),[27] to link from above the analyte already captured by a plasmonic surface. The latter consisted of 30 nm diameter AuNPs densely packed on a glass substrate (300 ± 20 AuNPs per µm^2) via the electrostatic self-assembly technique.[28,29] The AuNPs were functionalized using the photochemical immobilization technique (PIT), a method developed by our research group.[30,31] This technique relies on the selective UV activation of antibodies (Abs) and is characterized by its rapid, user-friendly nature. It results in the formation of robust covalent bonds between Abs and the sensor surfaces, with the Abs conveniently oriented for enhanced performance. An additional pivotal aspect in the biosensor's development was the integration of a fluidic system with the plasmonic substrate.[32] This integration proved crucial, as the fluidic device was specifically designed to accommodate a plasmonic device with metal structures facing the flow. Such a design facilitated enhanced interaction of antibodies, as well as other solutions such as BSA and analytes, on the nanostructured surface. By minimizing the volume of solutions employed, the biosensor achieved a homogeneous surface coverage, contributing significantly to its overall efficiency and reliability. Utilizing an external magnetic field enabled a controlled and targeted delivery of the top bioreceptor, facilitating specific binding to the target analyte and accelerating the detection time, thereby overcoming passive diffusion. The detection of target analyte led to a change in the extinction spectrum of the immunosensor, exhibiting features more similar to the spectrum of CSMPs as the analyte concentrations increased. With a simple and robust colorimetric response, the immunosensor demonstrated its capability to detect a specific protein involved in the immune response at low concentrations on the order of a few hundred pg mL^{-1} within minutes.

2. Results

2.1. Characterization of CSMPs

The CSMPs were synthetized by reacting tetrachloroauric acid ($HAuCl_4 \cdot 3H_2O$) with positively charged PEGylated dextran iron oxide composite particles (positively charged MNP clusters) in the presence of a reducing agent, the sodium citrate.[18] This last one played a role in inducing acid reduction to generate gold seeds. Subsequently, as gold grew around the seeds, negatively charged citrate-capped AuNPs were assembled onto the positively charged MNP clusters, resulting in the formation of CSMPs. Additionally, the citrate-capped AuNPs negatively charged the CSMPs giving them the repulsive force that avoids the self-aggregation phenomena.[27] The CSMPs and their precursors underwent thorough characterization using various techniques. Transmission electron microscopy (TEM) revealed the irregular shape of the MNP clusters, along with the presence of smaller AuNPs on the CSMPs surface, measuring approximately 15–20 nm in diameter (**Figure 1**a). Dynamic light scattering (DLS) was utilized to assess the overall size of the nanoconstructs. In Figure 1b, the size distribution of MNP clusters (depicted by the yellow line) and CSMPs (indicated by the purple dashed line) in ultrapure water is illustrated. The hydrodynamic diameter of bare MNP clusters peaked at ≈250 ÷ 260 nm, while CSMPs exhibited a peak at ≈350 ÷ 450 nm, attributed to the presence of the AuNPs coating. The formation of CSMPs was further confirmed through zeta potential measurements. In water, the ζ-potential distribution peaked at −38 mV for CSMPs, as illustrated by the purple dashed line in Figure 1c, compared to ∓30 mV for bare MNP clusters indicated by the yellow line. A ζ-potential value beyond −30 mV indicates high colloidal solution stability, confirmed by their usability several weeks after synthesis.[33] CSMPs exhibited a saturation magnetization of 51 emu g^{-1}, slightly lower than the 55 emu g^{-1} observed for MNP clusters (refer to Figure 1d, purple dashed and yellow lines, respectively). This deliberate reduction in saturation magnetization (10%) was successfully achieved in our investigation. The fragmented gold coating, as opposed to a uniform coating, distinguishes CSMPs as a preferable option over fully coated MNPs. This configuration ensures the absence of a "heavy" diamagnetic layer, allowing the retention of the initial magnetic properties. The presence of AuNPs on the surface of MNP clusters was confirmed through spectroscopic measurements. In Figure 1e, the experimental extinction spectra of MNP clusters (yellow line) and CSMPs (purple dashed line) are displayed. MNP clusters exhibited no extinction peak, while CSMPs showed a prominent resonance at ≈554 nm, confirming the existence of AuNPs and the successful synthesis of CSMPs. The gold growth on MNP clusters is visually apparent, as it results in a color change in the colloidal solution from light brown to burgundy red (Figure 1f). The magnetic core facilitates rapid particle collection (≤1 h for 20 mL CSMPs colloidal solution) under an external magnetic field generated by a permanent magnet (axially magnetized NdFeB with a thickness of 9 mm, a diameter of 20 mm, and a residual induction of 1.32 T) as depicted in Figure 1f.

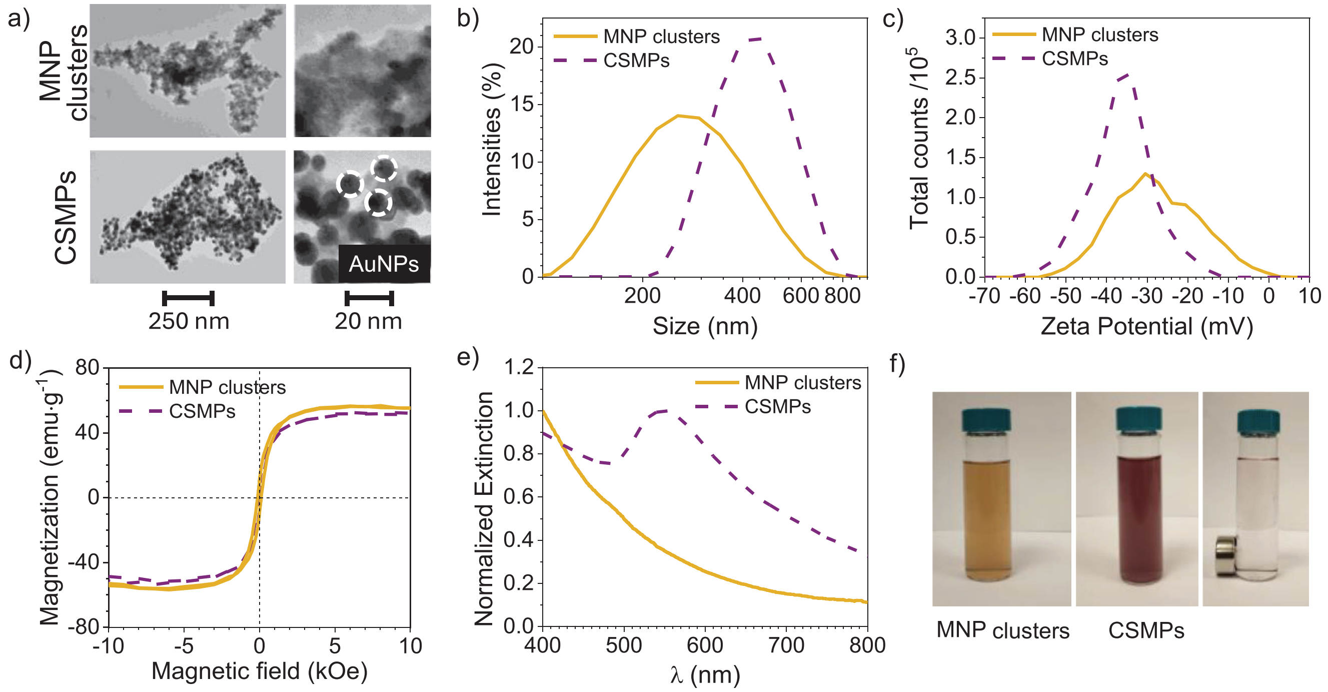

Figure 1. Characterization of CSMPs. a) TEM images of MNP clusters (top view) and CSMPs (bottom view). The circled area highlights the AuNP on MNP cluster. b,c) DLS and ζ-potential of MNP cluster (yellow line) and CSMPs (purple dashed line). d) Specific magnetization of CSMPs (purple dashed line) of 51 emu g^{-1} with respect to 55 emu g^{-1} for MNP clusters (yellow line). e) The extinction spectra of the MNP clusters (yellow line) do not exhibit any extinction peak, whereas the spectrum of the CSMPs shows a prominent resonance at ≈554 nm (purple dashed line). f) Photograph of the colour change of the colloidal solution from light brown to burgundy red as a result of the AuNPs on MNP clusters. Magnetic separation of CSMPs in water occurs in $\leq$ 1 h for 20 mL solution.

2.2. Characterization of AuNPs Surface

The nanostructured gold surface was created through the electrostatically driven self-assembly technique.[28] This method relied on the spontaneous adsorption of pre-synthesized citrate-capped AuNPs,[34] carrying a negative charge, onto a positively charged glass substrate through electrostatic interactions. The AuNPs surface was morphologically characterized by scanning electron microscopy (SEM). In the SEM micrograph at low magnification, spheroidal NPs were observed, randomly distributed onto the substrate as both single particles and clusters (**Figure** 2a). The image displayed a very high AuNPs surface density of ≈300 AuNPs μm^{-2}, ensuring a large number of binding sites available for immobilizing the bioreceptors. The spheroidal AuNPs could be approximated as spheres, and a narrow Gaussian distribution for their diameters with mean value $\langle D \rangle = (33 \pm 7)$ nm was obtained (Figure 2c). Finally, Figure 2d shows the histogram of the nearest-neighbor center-to-center distances, with a distribution having a mean value $< d > = (38 \pm 8)$ nm. The nanostructures were also optically characterized through UV–vis spectroscopy by measuring the extinction spectrum. Figure 2b shows the experimental extinction spectrum of the nanostructure (black line), featuring a plasmonic resonance at 528 nm and a "shoulder" in the range 600–800 nm. The former was associated with both single AuNPs far enough from their nearest neighbors to be considered as isolated, and AuNPs close enough to mildly interact with each other. Instead, the shoulder was associated with AuNPs in proximity, forming clusters that interact with longer wavelengths due to their larger overall size.

2.3. Functionalization and Analyte's Recognition of AuNPs Surface

Functionalization of the plasmonic surface and analyte capture were carried out using a model antibody–antigen pair—anti-human IgG and human IgG—to optimize detection efficiency protocols. Importantly, the results obtained can be readily extended to any other antibody-antigen IgG pair. The AuNPs surface was functionalized using a fluidic setup that incorporated a peristaltic pump with a 3D printed fluidic cell (**Figure** 3a). The fluidics was custom-designed to match the geometry of the plasmon nanostructure, resembling a multiwell plate with eight cylindrical-shaped cells. The fluidic geometry gave rise to a circular well on the AuNPs surface. This well was subsequently functionalized to enable detection. Moreover, the cells were connected in a series circuit, allowing for the simultaneous execution of at least three different experiments. The bottoms of the cells were attached to the plasmonic surface with a silicone O-ring, preventing charge loss of solutions. The O-ring created a sort of swimming pool with a volume of 30 µL, facilitating efficient interaction between the solution and the gold surface. Moreover, the fluidics ensured the uniform distribution of samples and reagents across the sensing area, guaranteeing consistent and reliable

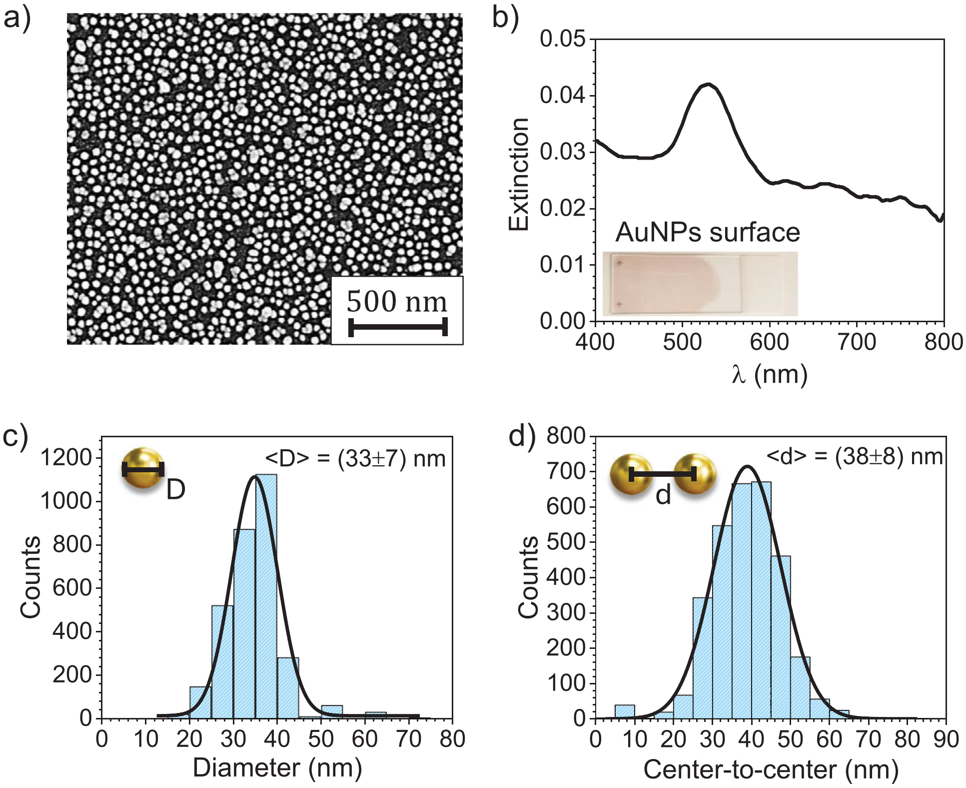

Figure 2. Characterization of the AuNPs surface. a) SEM micrograph of the 2D AuNPs array from a top view. b) The extinction spectrum of AuNPs surface, indicating a plasmon resonance at 528 nm. The inset features a photograph of the plasmonic nanostructure. c) Distribution of nanoparticle diameters. d) Distribution of the center-to-center distances.

measurements while minimizing variations due to manual handling.[35] A volume of 1 mL of Abs solution in PBS activated by PIT, flowed onto the plasmonic surface. The concentration of Abs was fixed to 2.5 µg mL^{-1}, ensuring a red-shift of approximately 6.5 nm (Figure 3b). The fluidic cells facilitated the flow of other solutions, such as BSA and analyte, over the plasmonic surface. While the functionalization process resulted in a red-shift and an increase in the extinction spectrum of the AuNPs surface due to an increased refractive index of the surrounding environment, no discernible changes were observed when the analytes bound to the antibodies. This is true even at a relatively high target concentration (100 ng mL^{-1}), as illustrated in Figure 3b. This

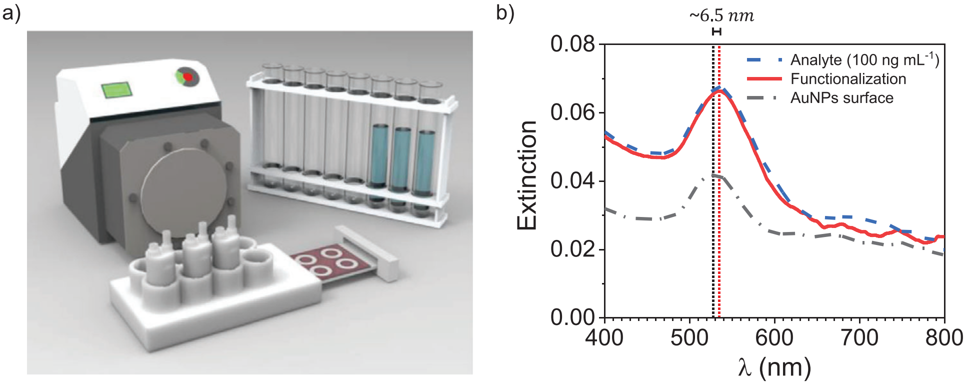

Figure 3. Fluidic setup. a) The AuNPs surface is placed within a custom 3D-printed multi-well plate, sealed from above with cylindrical-shaped cells. The geometry of the fluidic setup constrains the circular well on AuNPs surface, which is subsequently functionalized for the detection of PTX3. Biological samples circulate onto the AuNPs surface by using a peristaltic pump. b) The red-shift and the increase in the extinction spectrum of the plasmonic surface after the functionalization process (red line), compared to the bare AuNPs surface (dash and point black line), are due to a layer of Abs surrounding the NPs. On the other hand, the antibody-analyte binding (dashed blue line superimposed on red ones) does not produce any appreciable variation, underlining the need to use amplifiers.

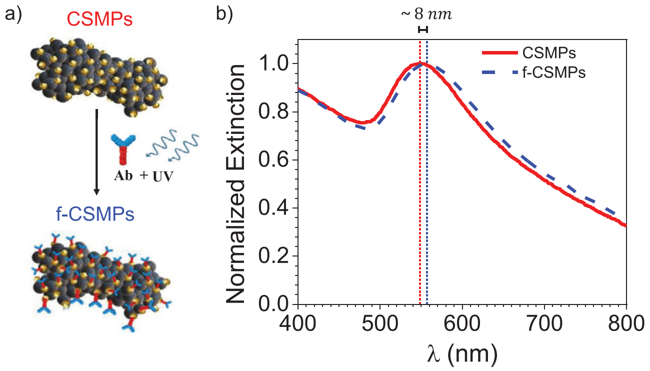

Figure 4. CSMPs functionalization process. a) Antibodies are immobilized on the gold surface using PIT, based on the selective UV activation of Abs. b) Extinction spectrum of CSMPs (red line) and CSMPs after the functionalization process (f-CSMPs, blue dashed line). A red-shift of ≈8 nm of the extinction spectrum of f-CSMPs is attributed to an increase in the refractive index of the environment surrounding the AuNPs.

observation underscored the essentiality of employing CSMPs as amplifiers.

2.4. CSMPs Functionalization

The functionalization of CSMPs for use as amplifiers involved the application of PIT,[31] to enable the covalent attachment of anti-human IgG Abs specific to the target analyte on the AuNPs. This process included activating a solution of Abs (100 µL at 12.5 µg mL^{-1}) with PIT and manually adding this activated Ab solution to 1 mL of CSMPs.

The formation of an Abs layer around the AuNPs surface entailed an increase of the local refractive index, leading to a red-shift of the resonance peak position. **Figure 4** shows the result of the CSMPs functionalization process, showing an ≈ 8 nm red-shift in the extinction spectrum of the functionalized CSMPs (f-CSMPs).

2.5. Enhancement of Optical Response on AuNPs Surface by f-CSMPs

The biosensor employed a sandwich scheme, illustrated in **Figure 5a**, where f-CSMPs bound from above the analyte already immobilized on the functionalized AuNPs (f-AuNPs) surface. The application of an external magnetic field by an axially magnetized NdFeB permanent magnet, whose characteristics are provided in Section 2.1, significantly enhanced the detection time, overcoming passive diffusion. Specifically, the magnet-driven detection time was reduced to 2 min, a substantial improvement compared to hours required for diffusion-driven motion. In Figure 5b, the extinction spectrum of the immunosensor is presented for a relatively high analyte concentration of 100 ng mL^{-1}, recorded after only 2 min of exposure to the magnetic field. Notably, changes in the extinction spectrum were observed during detection, exhibiting features more closely resembling the CSMPs spectrum as analyte concentrations increased. To enhance the spectra differences, the data were normalized, and ΔArea was chosen as the sensing parameter, representing the difference between the area after detection (post-CSMPs incubation) and the area before, Figure 5c.

We conducted initial tests on the immunosensor response with and without the magnet. As depicted in Figure 5d, in the absence of the magnetic field, approximately an hour was required for the biosensor response to significantly deviate from the control experiment (performed without the analyte but with the application of an external magnetic field). However, even without the magnetic field, the response remained lower than the experiment conducted with the magnet, as indicated by the yellow blocks in comparison to the red ones. On the other hand, the experiment confirms that a 2 min application of the magnetic field is sufficient to attract all CSMPs towards the plasmonic surface. The biosensor's response remained consistent, whether waiting for 2 min or 1 h. To determine if the analyte surface was saturated, we conducted the experiment in Figure 5e. In this case, the CSMPs solution on the substrate was refreshed every 2 min. The outcome indicated that a total of 6 steps, each lasting 2 min, were required to fully saturate the surface.

2.6. PTX3 Detection

The optimized protocol has been employed to detect pentraxin3 (PTX3) [36,37] in PBS, a protein involved in innate immune responses and inflammatory processes. The experiment involved varying PTX3 concentrations from 250 pg mL^{-1} to 100 ng mL^{-1}. For a better visualization, **Figure 6a** shows the extinction spectra at selected PTX3 concentrations—100, 50, 10, 1 ng mL^{-1}—alongside a control performed under the same conditions but without analyte. Figure 6b showcases the normalized spectra, and the dose-response curve is reported in Figure 6c. The experimental data were fitted by a logistic curve:

$$y = A_2 + \frac{A_1 - A_2}{1 + \left(\frac{x}{x_0}\right)^p} \tag{1}$$

with $A_1 = 0.26 \pm 0.02$, $A_2 = 1.34 \pm 0.03$, $x_0 = 3.33 \pm 0.28$, $p = 1.49 \pm 0.17$, and a $\tilde{\chi}_o^2 = 1.5$.

Applying the $3\sigma_{\text{mean}}$ criterion (shaded area in Figure 6c), we achieved a limit of detection of 300 pg mL^{-1}. To assess the specificity of the immunosensor, the sensor's response has been measured to detect different types of proteins involved in the inflammatory response, interleukin 6 and 8 (IL-6 and IL-8), by employing the same experimental procedure used to detect PTX3. In the most challenging scenario, we employed the immunosensor to identify IL-6 and IL-8 at the upper limits of protein concentrations detectable, 100 ng mL^{-1}. Figure 6d highlighted that signals acquired from analytes different from PTX3 were comparable with the control signal range. Importantly, these signals notably differed from those obtained for PTX3 at equivalent concentrations.

3. Conclusions

In this work, we demonstrated that the CSMPs enhance the optical response of a nanostructured gold surface. The CSMPs were

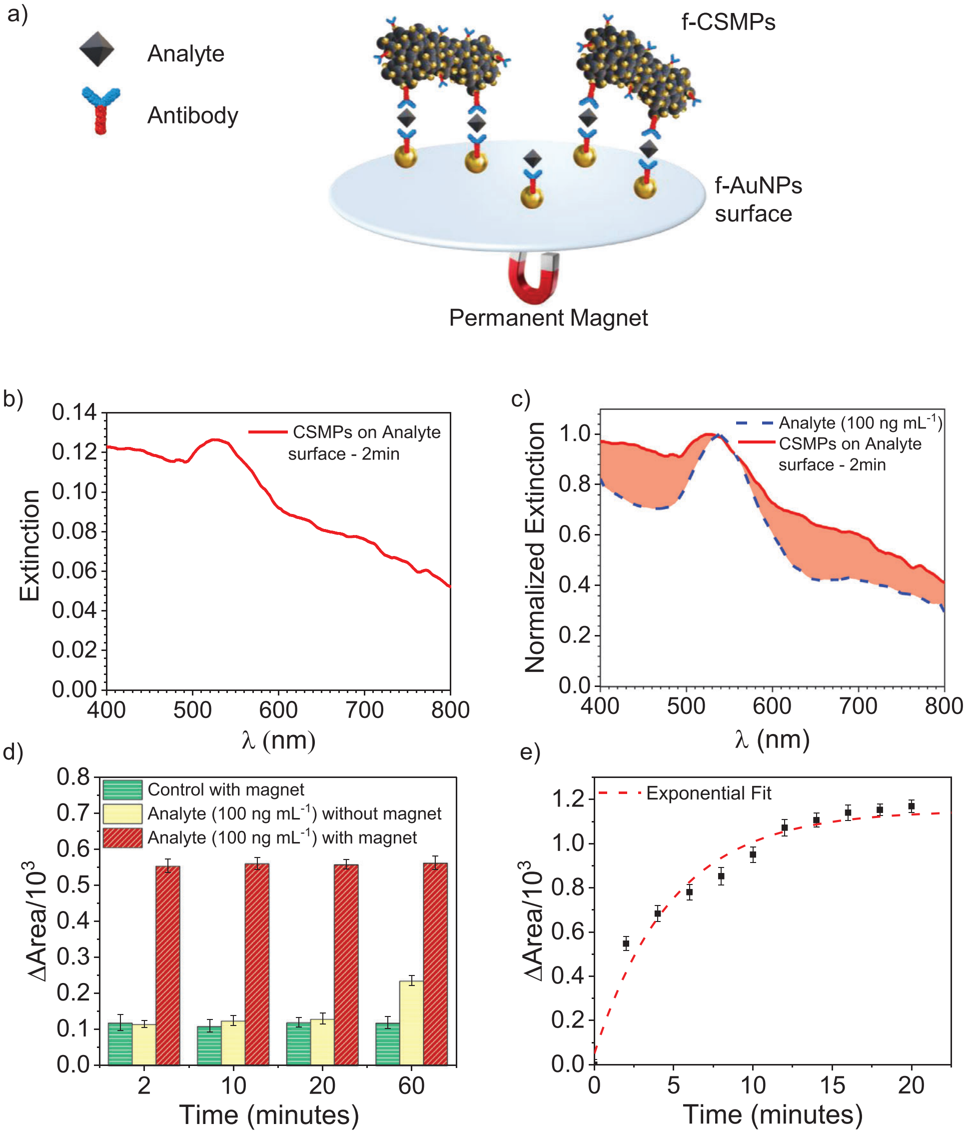

Figure 5. Immunosensor sandwich scheme and response. a) f-CSMPs bind from above to the analytes, which are already immobilized on the f-AuNPs surface, in the presence of an external magnetic field. b) Extinction spectrum measured at an analyte concentration of 100 ng mL^{-1}. Its shape results from the combination of f-CSMPs and f-AuNPs spectra. c) ΔArea (the region depicted in red) is the increase of the (normalized) area due to f-CSMPs binding and was used as the sensing parameter. d) Results of the experiment carried out by applying the magnet for only 2 min in presence and absence of the analyte (red and green bar, respectively). The yellow bar reports the results achieved with the analyte but without the magnet. While 2 min are enough to draw the CSMPs towards the substrate in presence of the magnetic field, one hour is barely enough to observe a small change of ΔArea when no magnetic field is applied (passive diffusion). e) The measurement of ΔArea was performed several times after the two-min interaction (followed by washing). The best fit of the experimental data with an exponential (dashed red line) provided a time constant $\tau = 5 \pm 1$ min corresponding to 2.5 cycles. To reach a value significantly close to saturation, 6 cycles was chosen for the measurement. In both the panels d) and e), the errors on ΔArea are derived from three independent measurements.

synthesized by inducing the growth of AuNPs directly onto the MNP clusters, enabling them to exhibit strong magnetization and high stability in a colloidal solution. The AuNPs covering enabled the use of the Photochemical Immobilization Technique to functionalize the CSMPs with antibodies, transforming them into immunoreactive particles characterized by a high magnetic response under external magnetic fields. Furthermore, we engineered a plasmonic nanostructure with a high density of AuNPs (30 nm diameter, 300 ± 20 AuNPs per μm^2), ensuring a substantial number of binding sites for the immobilization of bioreceptors. Antibodies were affixed to the gold surface using a custom 3D printed fluidic cell. Fluidics played a pivotal role in our biosensor development, facilitating precise control of the flow and ensuring the uniform distribution of samples and reagents across the sensing area. This uniformity not only guaranteed consistent and reproducible measurements but also minimized manual errors. Fluidics was also employed to guide the flow of BSA and analyte solutions over the nanostructured surface. The final

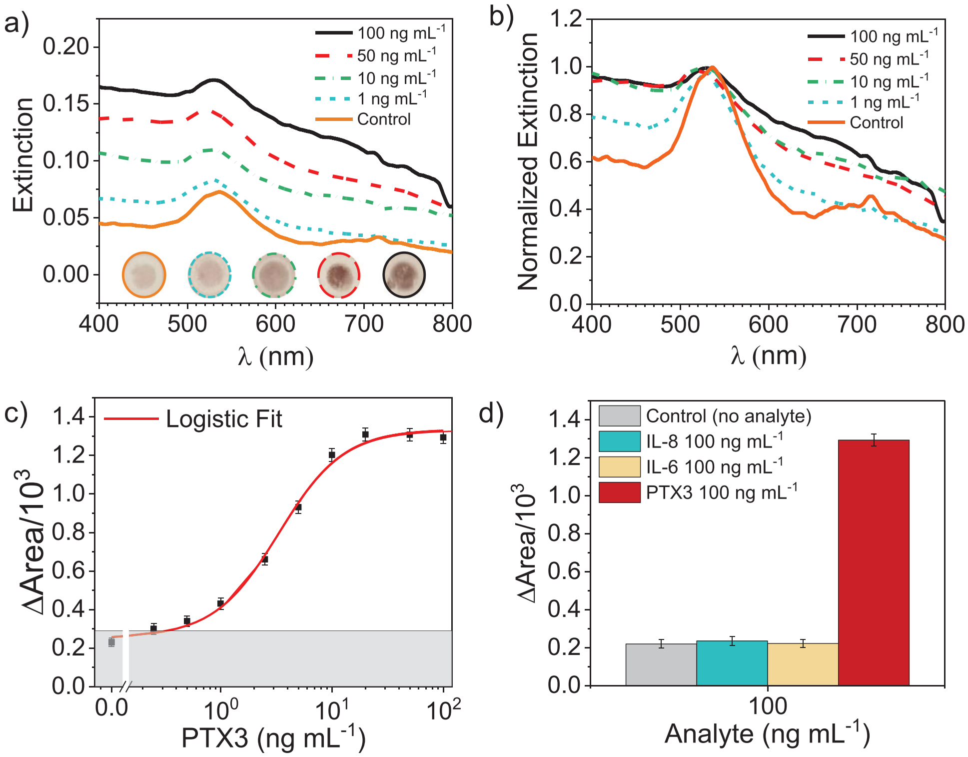

Figure 6. PTX3 detection. a) Extinction spectra of the immunosensor at some PTX3 concentrations— 100 ng mL^{-1} (black line), 50 ng mL^{-1} (red dashed line), 10 ng mL^{-1} (green dashed dot line) and 1 ng mL^{-1} (turquois short-dashed line). The control experiment (orange line) has been carried out in the same conditions but without analyte. The inset shows the images of the immunosensor wells taken as function of the PTX3 concentration, increasing from left to right. Each image is represented by a circle with the same line (style and color) used for the correspondent extinction spectrum. b) Normalized spectra enhance the differences at analyte concentrations. c) Dose–response curve for the detection of PTX3 in PBS. The experimental data were well fitted by a logistic function ($\tilde{\chi}_o^2 = 1.5$). d) Specificity test at different types of proteins (IL-6 and IL-8) at higher concentrations (100 ng mL^{-1}). c,d) ΔArea values are shown as "mean ± σ_{mean}", derived from three independent measurements ($n = 3$), with error bars indicating the standard deviation of the mean.

step, involving the binding of analytes by f-CSMPs, occurred statically. A small droplet of f-CSMPs was placed in the well on the AuNPs surface and was drawn downward by an external magnetic field. This magnetic field significantly enhanced the biosensor response and sensitivity, simultaneously reducing the detection time. Only 2 min were required to pull down all CSMPs towards the AuNPs surface, while a total of 6 steps, each lasting 2 min, was needed to saturate the analyte surface. Consequently, we were able to complete an experiment by measuring the target analyte concentration in less than 30 min. For the detection of PTX3 in PBS, the immunosensor achieved a limit of detection of about 300 pg mL^{-1}. Thanks to the simplicity of colorimetric measurements, our biosensor is well-suited for point-of-care applications. Its fluidic design not only allows for straightforward extension to multiplexing analysis but enables measurement in a controlled and clean environment through washing steps. Consequently, the actual extinction measurements are carried out in the absence of any possible nonspecific reactant present in the matrix. Thus, even with real samples, the effectiveness of our device is expected to be preserved. In summary, the integration of fluidics, coupled with the rapid biosensor response achieved through the magnetic properties of CSMPs described here, offers significant advantages, including improved sensitivity, reduced detection times, and enhanced throughput.

4. Experimental Section

Reagents and Materials: Milli-Q ultrapure water (resistivity 24 MΩ cm) was used for the preparation of all solutions. Tetrachloroauric acid ($HAuCl_4{\cdot}3H_2O$), sodium citrate ($Na_3C_6H_5O_7$), and bovine serum albumin (BSA) were supplied by the Sigma-Aldrich company (Milano, Italy). Pentraxin3 (PTX3) was purchased from Abcam company. Rabbit polyclonal antibody against pentraxin3 (GTX135596) were supplied by GeneTex. Phosphate Buffered Saline (PBS, 0.01 M, pH 7.4) was prepared by dissolving PBS tablets (from Gold Bio, St Louis, MO, USA) in Milli-Q water; each tablet prepared 100 mL of a 0.01 M PBS solution. The positively charged PEGylated dextran iron oxide composite particles (positively charged MNP clusters) were obtained from MicroMod (product name nanomag-D, product code 09-54-252). They possess a core-shell-like structure comprising a magnetite core and a dextran shell. The magnetite core consists of aggregates of individual iron oxide (magnetite) crystals with diameters ranging from 5 to 15 nm. The dextran surface of the particles has been modified with PEG 300 to prevent non-specific protein binding on the particle surface. The SuperFrost Plus Adhesion slides (25 × 75 × 1 mm) were purchased from Epredia. They feature a permanent positive charge on standard microscope slides that electrostatically attracts the negatively charged AuNPs. The instrumentation used for gold coating of NPs includes a mechanical motor stirrer (Heidolph RZR 50, Germany), hot plate (DLAB MS-H28- PRO), ultrasonic bath (Elma sonic S-40H 37 KHz), and spectrophotometer (Jenway 6715 UV/vis). N42-grade NdFeB magnets with a thickness of 9 mm and a diameter 20 mm were purchased from supermagnete.com.

Synthesis of CSMPs: The gold coating procedure, initially proposed by Silva et al.,[18] was refined by adjusting reagent concentrations and introducing a rapid cooling step to prevent undesired aggregation. The synthesis involved dissolving tetrachloroauric acid ($HAuCl_4 \cdot 3H_2O$) with positively charged PEGylated dextran iron oxide composite particles. In detail, a 25 mL of ultrapure water (Milli-Q) was heated to 100 °C with vigorous stirring using a mechanical motor stirrer (Heidolph RZR 50, Germany). After reaching the temperature, 34 µL of positively charged PEGylated dextran iron oxide composite particle (10 mg mL^{-1}), purchased from Micromod (Germany) with a diameter of 250 nm, were added. Then, 1.7 mL of sodium citrate at 10 mg mL^{-1} and 50 µL of $HAuCl_4 \cdot 3H_2O$ at 10 mg mL^{-1} were added to induce acid reduction and produce gold seeds, anchoring the PEG. Subsequently, due to gold growth around the seeds, negatively charged citrate-capped AuNPs were assembled onto the positively charged MNP clusters, resulting in the formation of CSMPs. Citrate molecules acted as both a reducing agent and capping agent, negatively charging the CSMPs and providing repulsive forces to prevent self-aggregation. The growth of gold on PEGylated dextran iron oxide composite particles induces a color change in the colloidal solution from light brown to burgundy red, which stabilizes within 15 min. Subsequently, the solution was cooled in ice maintaining the same stirring speed. To purify the CSMPs solution from excess reagents and products dissolved in the supernatant, an axially magnetized NdFeB magnet was employed. After magnetic separation, the particles were resuspended in 10 mL of Milli-Q water, resulting in a colloidal solution with a concentration of 5×10^9 CSMPs mL^{-1}. Furthermore, several batches of CMSPs were synthesized and analyzed using DLS. Consistency in the observed size distribution across all tested samples indicates the reproducibility of the synthesis protocol.

Synthesis of AuNPs: The AuNPs were synthesized following a Turkevich-modified protocol.[34] In a process, 0.5 mL of $HAuCl_4 \cdot 3H_2O$ (24×10^{-3} M) was mixed with 50 mL of ultrapure water and warmed on a hot plate at 150 °C with vigorous stirring. At boiling, 6 mL of sodium citrate dihydrate (($Na_3C_6H_5O_7$) at 39×10^{-3} M) was added to induce gold seeds formation. After 2 min, 4.2 mL of $HAuCl_4 \cdot 3H_2O$ (24×10^{-3} M) was added to promote particle growth. The solution's color transitioned from transparent to black and then to bright red within a few minutes. Afterward, the solution was cooled for 2 h by holding vigorous stirring. The synthesized AuNPs exhibited an extinction spectrum with a narrow peak at 528 nm and an Optical Density (OD) of 8, indicative of spherical AuNPs with an average diameter of 30 nm.

Fabrication of AuNPs Surface: The glass surface (SuperFrost Plus Adhesive slides) was cleaned with Milli-Q, and an airgun. Subsequently, it was immersed in an AuNP solution with OD 2 for 1 h. The pre-synthesized AuNPs were immobilized onto the glass surface through electrostatic interactions between the negatively charged citrate capping on AuNPs and the positively charged surface. After 1 h, the glass substrate was rinsed with Milli-Q water and then dried using an airgun.

Particle Characterization: DLS and zeta potential measurements were performed using the Zetasizer Nano ZS instrument from Malvern Instruments. TEM micrographs were obtained with an FEI Tecnai G2 S-twin apparatus operating at 200 kV and equipped with a LaB6 source. For TEM analysis, particle powder samples were dispersed in water, and a small quantity of the solution was applied onto a carbon-coated copper grid (200 mesh) and allowed to dry. The AuNPs surface underwent gold/palladium sputtering (30 s, 25 mA) for morphological characterization using SEM micrographs obtained with a Zeiss LEO 1550VP field emission scanning electron microscope (FESEM) at a nominal resolution of 1 nm and 20 kV acceleration voltage. UV–vis absorbance spectra were recorded on a Jenway 6715 UV/vis spectrophotometer within a spectral range of 400–800 nm with 0.1 nm resolution.

Antibodies Conjugation to CSMPs: The PIT was employed for the efficient immobilization of immunoglobulins on thiol-reactive surfaces, such as AuNPs. To functionalize the CSMPs solution, a volume of 100 µL of Abs solution—12.5 µg mL^{-1} in PBS—was placed in a quartz cuvette and exposed to UV light for 30 s, determined as the optimal irradiation time for PIT. Subsequently, the solution was introduced drop by drop into a 1 mL CSMPs solution at OD 1 under gentle stirring, ensuring proper mixing and dispersion of the functionalized antibodies within the CSMPs solution. To remove unbound Abs, the CSMPs underwent magnetic separation from the solution, a process lasting about 5 min. It is noteworthy that employing a Teflon beaker was essential to separate the CSMPs from excess antibodies and avoid particle adhesion to the glass beaker. The successful formation of an antibodies layer around the AuNPs resulted in a red-shift of ≈8 nm in the extinction spectrum of the CSMPs, a shift considered significant as the experiment's success criterion required LSPR shift greater than 5 nm.

Preparation of AuNPs Surface to the Analyte's Recognition: The functionalization of AuNPs surface involved several steps. The gold nanostructured surface was placed into the custom 3D printed multi-well plate and covered from above with a cylindrical-shaped cell. A volume of 1 mL of Abs solution at 2.5 µg mL^{-1} was activated by PIT and flowed onto the surface. The flow rate and the flowing time were set at 850 µL min^{-1} and 15 min, respectively. The flow time was chosen as a trade-off between the short time required by PIT (the produced thiol is effective for approximately 10 min) and the extended time needed to conserve Abs (as consumable material). Following this, a 5 min washing step with Milli-Q water was carried out to eliminate non-bonded Abs. Subsequently, BSA with a concentration of 5 mg mL^{-1} and the target analytes at different concentrations flowed onto the f-AuNPs for 15 min. After the analytes flowed, the surface underwent a 5 min wash in Milli-Q water.

PTX3 Detection: A 30 µL droplet of CMSPs conjugated with anti-PTX3, with an OD of 1 (containing 10^8 f-CSMPs), was carefully placed into the well on the nanostructured surface through which the PTX3 analyte had been circulated. The f-CSMPs were guided downward by a magnet positioned under the substrate for 2 min, the estimated time needed to draw all CMSPs toward the substrate. Following this, the surface underwent a rinse with Milli-Q water. The f-CSMPs incubation was repeated 6 times (as indicated by Figure 5e to saturate the analytes surface), and then, the extinction spectrum of the immunosensor was recorded. To facilitate this final step, a custom-designed 3D holder was meticulously crafted to precisely match the well on the nanostructure and can be easily inserted into the spectrophotometer. The extinction spectrum of the immunosensor changed accordingly to the analyte's concentrations, showing features more similar to f-CSMPs with increasing the PTX3 concentration.

Statistical Analysis: The extinction spectra of the immunosensor were normalized to their maxima to reduce fluctuations. In each plot, ΔArea values are shown as "mean $\pm \sigma_{mean}$", derived from three independent measurements ($n = 3$), with error bars indicating the standard deviation of the mean. The experimental data, describing ΔArea as function of analyte concentrations, were well fitted by a logistic function ($\tilde{\chi}_o^2 = 1.5$). Statistical analysis was carried out using Origin 9.5 Software.

Acknowledgements

The authors are grateful to Antonio Ramaglia for the helpful assistance in 3D printing.

Conflict of Interest

The authors declare no conflict of interest.

Author Contributions

M.D.L.: investigation, data curation, formal analysis, validation, writing original draft, and visualization. A. A.: formal analysis, methodology, data curation, validation, and visualization. D.M.: investigation, methodology, and validation. M.B.: resources, funding acquisition. D.I.: resources, funding acquisition. B.D.V.: conceptualization, supervision, methodology, writing review and editing. V.I.: conceptualization, resources, writing review, and editing. R.V.: supervision, project administration.

Data Availability Statement

The data that support the findings of this study are available from the corresponding author upon reasonable request.

Keywords

colorimetric immunosensor, core@satellite magneto-plasmonic particles (CSMPs), fluidic device, LSPR, pentraxin3, point-of-care diagnostics

Received: January 15, 2024
Revised: May 7, 2024

---

[1] M. Katagiri, J. L. Cuya Huaman, T. Matsumoto, K. Suzuki, H. Miyamura, J. Balachandran, *ACS Appl. Nano Mater.* **2020**, *3*, 418.
[2] H. Zhou, F. Zou, K. Koh, J. Lee, *J. Biomed. Nanotechnol.* **2014**, *10*, 2921.
[3] V. T. Tran, J. Kim, L. T. Tufa, S. Oh, J. Kwon, J. Lee, *Anal. Chem.* **2018**, *90*, 225.
[4] R. S. Singh, P. K. Sarswat, *Mater. Today Electron.* **2023**, *4*, 100033.
[5] Y. Chen, Y. Bai, X. Wang, H. Zhang, H. Zheng, N. Gu, *Biosens. Bioelectron.* **2023**, *219*, 114744.
[6] P. Singh, in *Reviews in Plasmonics*, (Ed: C. D. Geddes), Springer, Berlin **2017**, pp. 211–238.
[7] C. de Julián Fernández, F. Pineider, in *New Trends Nanoparticle Magnetism*, (Eds: D. Peddis, S. Laureti, D. Fiorani), Springer, Berlin **2021**, pp. 107–136.
[8] G. V. Hartland, *Chem. Rev.* **2011**, *111*, 3858.
[9] S. A. Maier, *Plasmonics: Fundamentals and Applications*, Springer, New York, NY **2007**.
[10] K. A. Willets, R. P. Van Duyne, *Annu. Rev. Phys. Chem.* **2007**, *58*, 267.
[11] C. Louis, O. Pluchery, *Gold Nanoparticles for Physics, Chemistry and Biology*, World Scientific, London **2017**.
[12] H. Aldewachi, T. Chalati, M. N. Woodroofe, N. Bricklebank, B. Sharrack, P. Gardiner, *Nanoscale.* **2018**, *10*, 18.
[13] V. Iannotti, V. Guarino, I. Cruz-Maya, Z. U. D. Babar, L. Lanotte, L. Ambrosio, L. Lanotte, *Sens. Actuators, A.* **2024**, *371*, 115272.
[14] L. Trahms, *Biomed. Tech.* **2015**, *60*, 389.
[15] A. Kostopoulou, A. Lappas, *Nanotechnol. Rev.* **2015**, *4*, 595.
[16] S. Mourdikoudis, A. Kostopoulou, A. P. LaGrow, *Adv. Sci.* **2021**, *8*, 2004951.
[17] J. Zhang, L. Mou, X. Jiang, *Chem. Sci.* **2020**, *11*, 923.
[18] S. Moraes Silva, R. Tavallaie, L. Sandiford, R. D. Tilley, J. J. Gooding, *Chem. Commun.* **2016**, *52*, 7528.
[19] T. T. Nguyen, F. Mammeri, S. Ammar, *Nanomaterials.* **2018**, *8*, 149.
[20] M. Mehdipour, L. Gloag, D. T. Bennett, S. Hoque, R. Pardehkhorram, P. Bakthavathsalam, V. R. Gonçales, R. D. Tilley, J. J. Gooding, *J. Mater. Chem. C.* **2021**, *9*, 1034.
[21] M. Soroush, W. Ait Mammar, A. Wilson, H. Ghourchian, M. Salmain, S. Boujday, *Biosensors.* **2022**, *12*, 799.
[22] Q. Zhang, L. Wu, T. I. Wong, J. Zhang, X. Liu, X. Zhou, P. Bai, B. Liedberg, Y. Wang, *Int. J. Nanomed.* **2017**, *12*, 2307.
[23] Y. C. Chen, Y. C. Chou, J. H. Chang, L. T. Chen, C. J. Huang, L. K. Chau, Y. L. Chen, *Analyst.* **2021**, *146*, 6935.
[24] S. Balaban Hanoglu, D. Harmanci, N. Ucar, S. Evran, S. Timur, *Magnetochemistry.* **2023**, *9*, 23.
[25] I. Gessner, J. H. Park, H. Y. Lin, H. Lee, R. Weissleder, *Adv. Healthcare Mater.* **2022**, *11*, 2102035.
[26] W. Perng, G. Palui, W. Wang, H. Mattoussi, *Bioconjugate Chem.* **2019**, *30*, 2469.
[27] R. Campanile, A. Acunzo, E. Scardapane, A. Minopoli, V. C. Martins, R. Di Girolamo, S. Cardoso, R. Velotta, B. Della Ventura, V. Iannotti, *ACS Omega.* **2022**, *7*, 36543.
[28] M. O. Stetsenko, S. P. Rudenko, L. S. Maksimenko, B. K. Serdega, O. Pluchery, S. V. Snegir, *Nanoscale Res. Lett.* **2017**, *12*, 348.
[29] N. Thomas, P. Sreekeerthi, P. Swaminathan, *Phys. Chem. Chem. Phys.* **2022**, *24*, 25025.
[30] B. D. Ventura, M. Gelzo, E. Battista, A. Alabastri, A. Schirato, G. Castaldo, G. Corso, F. Gentile, R. Velotta, *ACS Appl. Mater. Interfaces.* **2019**, *11*, 3753.
[31] B. D. Ventura, M. Banchelli, R. Funari, A. Illiano, M. De Angelis, P. Taroni, A. Amoresano, P. Matteini, R. Velotta, *Analyst.* **2019**, *144*, 6871.
[32] L. Niu, N. Zhang, H. Liu, X. Zhou, W. Knoll, *Biomicrofluidics.* **2015**, *9*, 052611.
[33] S. Bhattacharjee, *J. Controlled Release.* **2016**, *235*, 337.
[34] J. Turkevich, P. C. Stevenson, J. Hillier, *Discuss. Faraday Soc.* **1951**, *11*, 55.
[35] T. D'Aponte, M. De Luca, N. Sakač, M. Schibeci, A. Arciello, E. Roscetto, M. R. Catania, V. Iannotti, R. Velotta, B. Della Ventura, *Sens. Diagn.* **2023**, *2*, 1597.
[36] G. Lapadula, R. Leone, D. P. Bernasconi, A. Biondi, E. Rossi, M. D'Angiò, B. Bottazzi, L. R. Bettini, I. Beretta, C. Garlanda, M. G. Valsecchi, A. Mantovani, P. Bonfanti, *Front. Immunol.* **2022**, *13*, 933960.
[37] A. Doni, M. Stravalaci, A. Inforzato, E. Magrini, A. Mantovani, C. Garlanda, B. Bottazzi, *Front. Immunol.* **2019**, *10*, 712.